Insights into Photopolymerization at the Nanoscale Using Surface Plasmon Resonance Imaging

Amine Khitous, Lionel Lartigue, Julien Moreau, Olivier Soppera

RESEARCH ARTICLE

NANO · MICRO small
www.small-journal.com

Insights into Photopolymerization at the Nanoscale Using Surface Plasmon Resonance Imaging

Amine Khitous, Lionel Lartigue, Julien Moreau, and Olivier Soppera**

Near-field photopolymerization (NFPP) driven by surface plasmon resonance has attracted increasing attention in nanofabrication. This interest comes from the nanometer-scale control of polymer thickness, due to the confinement of the evanescent wave within a highly restricted volume at the surface. In this study, a novel approach using a multi-spectral surface plasmon resonance instrument is presented that gives access to real-time images of polymer growth during NFPP with nanometer sensitivity. Using the plasmonic evanescent wave for both polymerization and real-time sensing, the influence of irradiance, concentration of dye, and initiator are investigated on the threshold energy and kinetics of NFPP. How oxygen inhibition in the near field strongly affects photopolymerization is highlighted, more than in the far field.

1. Introduction

Electromagnetic field confinement and enhancement are outstanding properties of plasmonic materials, that is, thin metallic films or nanoparticles (NPs). Precisely, at their surfaces, the incident electromagnetic field experiences significant subwavelength confinement[1–6] and irradiance enhancement, typically on the order of 10 to 100-fold, through the excitation of the surface plasmon evanescent wave.[2,5] These properties lead to interesting applications for sensors, photocatalysis, or nanofabrication. In particular, near-field photopolymerization (NFPP)[2,3,7,8] developed in recent years by several teams has shown potential for initiating spatially confined chemical reactions at the nanoscale. This corresponds to the ultimate resolutions for photo-assisted techniques. For example, work by Ge et al has demonstrated the possibility of integrating a single quantum spot into a nanoscale polymer lobe.[8] Moreover, this polymer lobe was localized at the nanoscale in a particular site on a nano-object thanks to polarization control. The work of Kameche et al focused on living NFPPs to control the functionalization of single NPs.[3] Khitous et al used this method to integrate polymer-based molecular imprints on gold NPs for sensing purposes.[6,9] Finally, Chegel et al[10] demonstrated the possibility of using the Surface Plasmon Evanescent Wave for polymerizing polymer film with thickness down to tens of nanometers. These examples show the interest and variety of materials that can be coupled to metal nanostructures using the NFPP approach. However, the kinetics of NFPP have, as yet, only rarely been studied, with the exception of the work of Deeb et al, who analyzed the effects of irradiation dose on polymer thickness in NF using atomic force microscopy.[11] In a recent study, NFPP kinetics were investigated in the LSPR configuration using UV-visible spectroscopy.[7] In this paper, we aim to study the specificities of NFPP compared to the well-established macroscopic photopolymerization processes using an innovative multi-spectral Surface Plasmon Resonance Imaging (SPRI) instrument to film, in real-time, the polymer growth at the nanoscale, with nanometers thickness resolution and measure photopolymerization kinetics. Our configuration is similar to the one used by Chegel et al with an added imaging capability.[10] Surface plasmons are extremely sensitive to refractive index (RI) changes occurring in the close vicinity of the metallic surface.[12,13] The normal spatial extension of the evanescent wave on a gold film in the visible spectrum is typically around 200 nm.[16] It depends on factors such as wavelength, metal properties, and the RI of the surrounding medium. Given its high sensitivity and imaging capabilities, Surface Plasmon Resonance imaging proves to be a very relevant choice for the study of NFPP. The latter can be continuously monitored through real-time measurements of the reflected beam on the surface of the gold film, giving the kinetic of photopolymerization with nanometer resolution in thickness.[14] To completely avoid thermoplastic effects and hot electron transfert[2] and only measure photoinduced polymerization, we have chosen in this study to use mild irradiation conditions. This is further justified by the fact that the confinement of the

A. Khitous, O. Soppera
Université de Haute-Alsace
CNRS
IS2M UMR 7361, Mulhouse F-68100, France
E-mail: olivier.soppera@uha.fr
A. Khitous, O. Soppera
Université de Strasbourg
Strasbourg F-67081, France
L. Lartigue, J. Moreau
Université Paris-Saclay
Institut d'Optique Graduate School, CNRS
Laboratoire Charles Fabry
Palaiseau 91120, France
E-mail: julien.moreau@institutoptique.fr

The ORCID identification number(s) for the author(s) of this article can be found under https://doi.org/10.1002/smll.202401885

DOI: 10.1002/smll.202401885

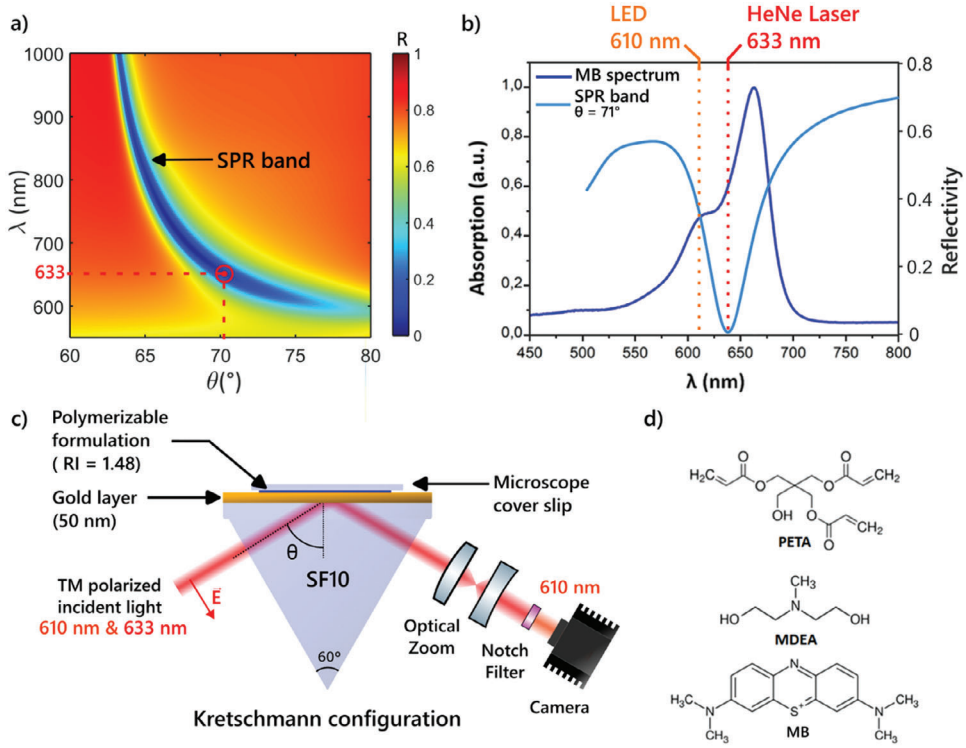

Figure 1. a) Normalized TM reflectivity map calculated as a function of the internal angle and wavelength for the studied configuration. b) UV–visible spectrum of F_{633} and surface plasmon spectral resonance for $\theta = 71°$. c) Simplified schematic showing the gold chip covered with the polymerizable formulation in a Kretschmann configuration. The photopolymerization is performed at a wavelength of 633 nm and monitored at a wavelength of 610 nm. d) Structures of molecules composing the formulation F_{633}.

evanescent wave on a gold film is less than what can be achieved around NPs.

In this article, we present the multi-spectral SPR imaging instrument used, and the formulation specially developed for NFPP. We then carry out an in-depth analysis of the NFPP reaction, particularly the influence of incident irradiance, the effect of photoinitiator (PI) concentration, and the role of oxygen diffusion as an inhibitor and its impact on polymer growth.

2. Results and Discussion

The Kretschmann configuration requires resonance conditions on the illumination to excite the surface plasmon.[16] Under the right wavelength and angle conditions, coupling between incident light and the surface plasmon occurs. To illustrate this phenomenon, the normalized Transverse Magnetic (TM) reflectivity of a gold film at different wavelengths and incident angles can be simulated using Fresnel reflection and transmission coefficients[17](**Figure 1a**). The reflectivity has been calculated as a function of wavelength and external angle of incidence for an SF10 prism coated with a 50 nm thick gold film covered by the polymerizable formulation with an RI of 1.48 measured using an Abbe refractometer. To trigger photopolymerization with surface plasmon, the SPR excitation band and PI absorption band must overlap. Thereby, the energy transfer of the electromagnetic field, which is enhanced through surface plasmon excitation, to the polymerizable formulation is maximized. Accounting for the excitation conditions of surface plasmon for the studied configuration, MB, having an absorption band centered at 665 nm (Figure 1b) is a good candidate. At a wavelength of 633 nm, an internal incident angle of 71° satisfies the resonance conditions. As explained above, monitoring of NFPP will be carried out using a second wavelength beam at 610 nm. It is important to note that in the Kretschmann configuration, the formulation is irradiated only in the near field through the surface plasmon evanescent wave. The entire volume of the formulation is not irradiated which is a major difference compared with the irradiation conditions used in previous studies carried out in the LSPR configuration, in the vicinity of metallic NPs.[2,7,9]

Figure 1d details the constituents of the F_{633}. It comprises PETA as a monomer (RI = 1.48), and a PI system consisting of a mixture of MB and MDEA. The molar ratio of the three molecules (MB:MDEA:PETA) is 1:24:358. This formulation undergoes photopolymerization according to a "Norrish II " mechanism[11] as shown in **Figure 2**. The initiation process takes place in two steps[11]: first, excitation of the dye (MB) to the electronically excited state S_1, then T_1 by intersystem conversion, followed by a reaction between MB^{T*} and MDEA, leading to the formation of free radicals $R^{\bullet}$ and $MBH^{\bullet}$. This step is highly sensitive to the presence of oxygen, which can inhibit the excited state of MB^{T*} by energy transfer, or convert the radicals ($R^{\bullet}$) and growing chains ($MR^{\bullet}$) into non-reactive species for polymerization (peroxides).[11] To limit the impact of oxygen, a glass slide is used on top of the sample. It prevents the renewal of oxygen from the atmosphere for the duration of the experiment.

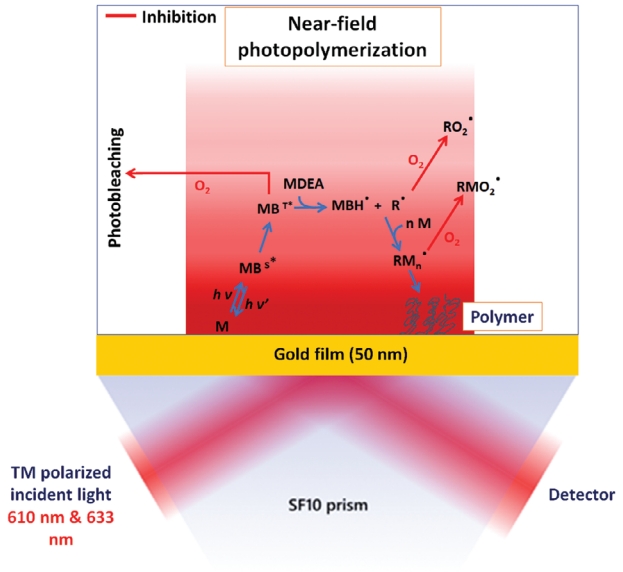

Figure 2. Schematic showing the mechanism of F633 SPR NFPP in Kretschmann configuration.

The plasmonic evanescent field at the surface of the gold film has an exponential profile over a few hundred nanometers above the surface. Using an open-source modal Fourier method electromagnetic model,[18,19] we calculated the enhancement factor, defined as the irradiance at a given height z above the gold film divided by the incident irradiance, in a medium of RI = 1.48 (F_{633}) and for different concentrations of MB in the formulation (**Figure 3**). The irradiance enhancement factor on the non-irradiated side of the film (z = 50 nm), reaches a maximum value of 17. A factor of 1 (no enhancement, defining the extension of the plasmonic evanescent wave) is reached at 205 nm from the gold surface. A 10 mM concentration leads to a 33% reduction of the intensity enhancement factor at the gold surface, due to the attenuation effect of MB at 633 nm. For the typical concentrations of MB used in this study (between 2 and 17 mM), the loss in enhancement factor is at most a factor 2. This is a worst-case scenario as the simulation assumed a homogenous MB concentration. Realistically, MB concentration will decrease near the surface as photopolymerization takes place.

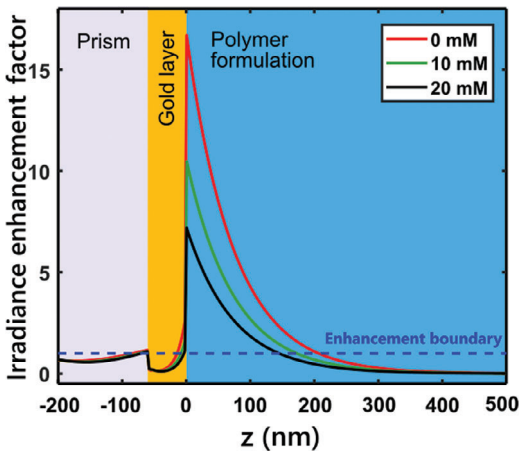

Figure 3. Simulation of irradiance enhancement factor through resonant surface plasmon excitation on a gold film (50 nm) surrounded by the polymer formulation for different MB concentrations.

To illustrate SPR photopolymerization for the F_{633}, a drop of the formulation was deposited on a gold film and irradiated at 633 nm with a 1 mm diameter beam and an intensity, before exaltation, of 6.4 W m^{-2} for six irradiation times from 80 to 180 s.

Figure 4a shows a photo of the gold film with the polymer spots obtained for the different irradiance times. White light interferences inside the polymer films are responsible for the colors observed. Qualitatively, we see an increase in polymer spot diameter and thickness with irradiation time. This was confirmed by profilometry (Figure 4c) with the thickness of the spots increasing from 100 nm up to 195 nm for the longest irradiation time. The major advantage of SPRI is that it gives real-time, quantitative reflectivity images of the polymerization process. Using an RI of 1.52[7] for the polymer, the reflectivity signal on each pixel can be converted into a polymer thickness using a generalized multilayer model.[20] Figure 4b shows such a reconstruction of all spots at the end of the polymerization process. This reconstruction can be done using the reflectivity images recorded during the irradiation (the film showing the real-time polymer growth in the near field is shown in Figure S3, Supporting Information) or after cleaning the sample and filling the fluidic cell with deionized water. Increasing the refractive index contrast between the polymer and the surronding medium significantly improves the precision of the calculated polymer thickness as the uncertainty on the polymer RI has less impact on the calculation. The dimensions derived from reflectivity measurements and transposed into thickness show good agreement with the profilometry measurements. It illustrates the value of the SPRI technique to give a precise insight of the temporal evolution of the optical thickness during the polymerization. As shown in Figure 4d, it is also possible to follow NFPP kinetics by looking at the reflectivity variation in a region of interest at the center of the spot, as a function of time. The polymer growth can be canceled, at the nanoscale, just by switching off the laser light. Furthermore, for the longest irradiation time, NFPP kinetics exhibits 3 distinct regimes. First, during a period of inhibition, the radicals formed but react with the oxygen present in the medium, preventing polymerization from starting; no change in reflectivity is observed. Then, when enough inhibitor is consumed in the illuminated near-field volume, polymerization begins efficiently, resulting in a rapid change in reflectivity. Finally, a plateau is reached when the polymerization spontaneously stops at a given distance from the gold surface where the evanescent wave intensity is too low (Figure 3). Using these tools, we have carried out an in-depth parametric study of NFPP, focusing on two key parameters: irradiance and PI concentration. By varying these parameters, we aim to understand how they influence the kinetics of SPR-induced NFPP. This will help optimize experimental conditions of plasmon-induced polymerization and have a better understanding of the mechanisms involved in the process. However, it is worth noting that alongside the chemical and physical parameters tested, the most widespread strategy to prevent oxygen diffusion from the atmosphere into the polymerizing

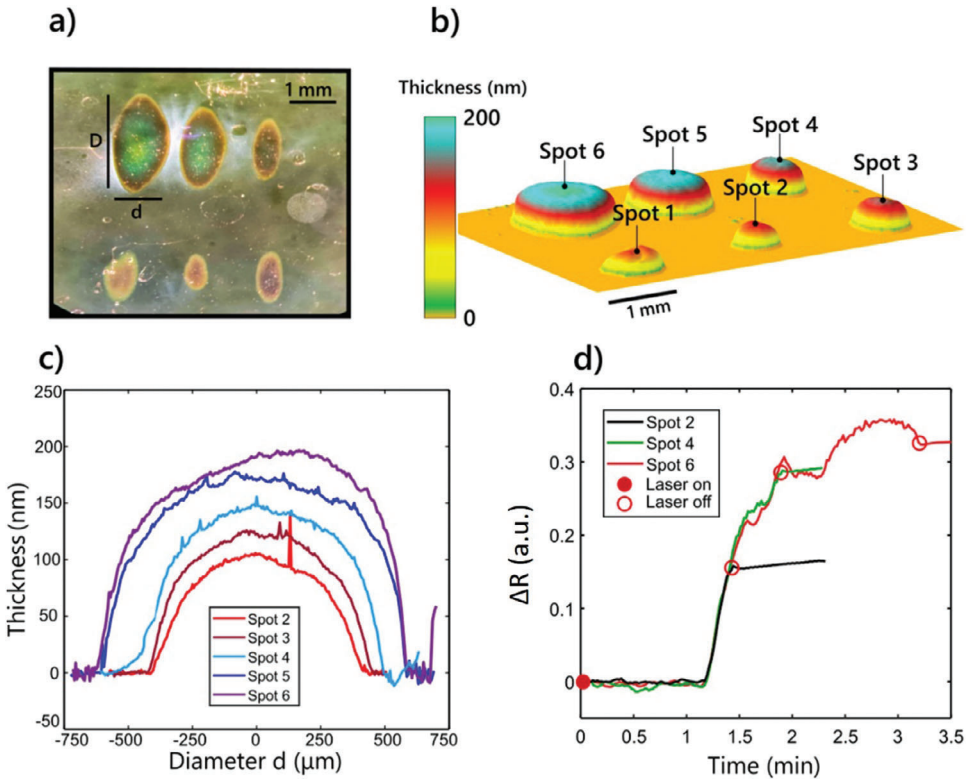

Figure 4. a): photo of the gold slide surface after NFPP. b) 3D reconstructed image from SPR data of the different spots obtained by NFPP for increasing irradiation times, c): profiles of 5 spots measured with a profilometer d) NFPP kinetics of spots N°2,4 and 6 for an incident intensity of 6.4 W m^{-2}. For clarity, the starting time of the kinetics curves has been superposed.

resin is blanketing with an inert gas.[21] In this study, we focus solely on the effect of irradiance and polymer concentration to investigate the NFPP kinetics.

2.1. Effect of Irradiance

A drop of F_{633} was deposited on the gold surface and protected by a glass slide as in the previous experiment. It was then irradiated using He-Ne laser light for different irradiances and for an angle of incidence of 71°, corresponding to the resonance conditions at 633 nm (Figure 1a).

Monitoring the NFPP reaction at different incident irradiances revealed, as expected, faster polymerization with increasing irradiance, as illustrated in **Figure 5**a. For the lowest irradiance (1.3 W m^{-2}), the NFPP threshold time was 15 min, meaning that during the first 15 min, the radicals formed are consumed by the oxygen. When irradiance is increased to 3.2, 6.4, and 17.8 W m^{-2}, the threshold times are reduced to 4 min, 12, and 5 s, respectively. Note that in these experiments, the polymer film growth was not manually stopped but rather ceased spontaneously when its thickness exceeded the evanescent wave normal extension. This corresponds to a reflectivity variation slightly below 30% for all experimental conditions. Indeed, if the incident irradiance is high enough to trigger NFPP, the entire normal extension of the evanescent field is polymerized over time, resulting in a flat polymer spot. This leveling effect is interesting for applications in nanofabrication. The same kinetics can also be plotted as a function of incident energy as shown in Figure 5c,d. It highlights how the energy thresholds for polymerization increase as the irradiance decreases and oxygen renews to inhibit the NFPP reaction. On the other hand, at higher irradiances, although the total energy is reduced, it is delivered over a shorter period, enabling oxygen to be rapidly consumed in the near field where the polymerization takes place.

Using the imaging capability of the dual-wavelength SPRI instrument, the temporal evolution of the polymer spot diameter can also be extracted for different incident irradiance conditions (Figure 5b). Lower irradiances lead to smaller spots, as the lateral polymer growth is limited by O_2 diffusion from the edge of the irradiated zone. For a given irradiance, the final diameter is mainly determined by the distance from the center of the irradiated zone where there is an equilibrium between oxygen consumption and supply by diffusion. Note that for all irradiances, the surface area of the irradiated zone is identical and elliptical due to the high incidence angle (see Figure S4, Supporting Information). Finally, as previously mentioned, 3D profiles of the polymer spots during polymerization can be reconstructed by processing the 2D reflectance images acquired at regular time intervals (Figure 5c, Supporting Information).

From these kinetics, the polymerization threshold time as well as the polymerization rate K_v can be extracted from the reflectance curves and are plotted in **Figure 6**.

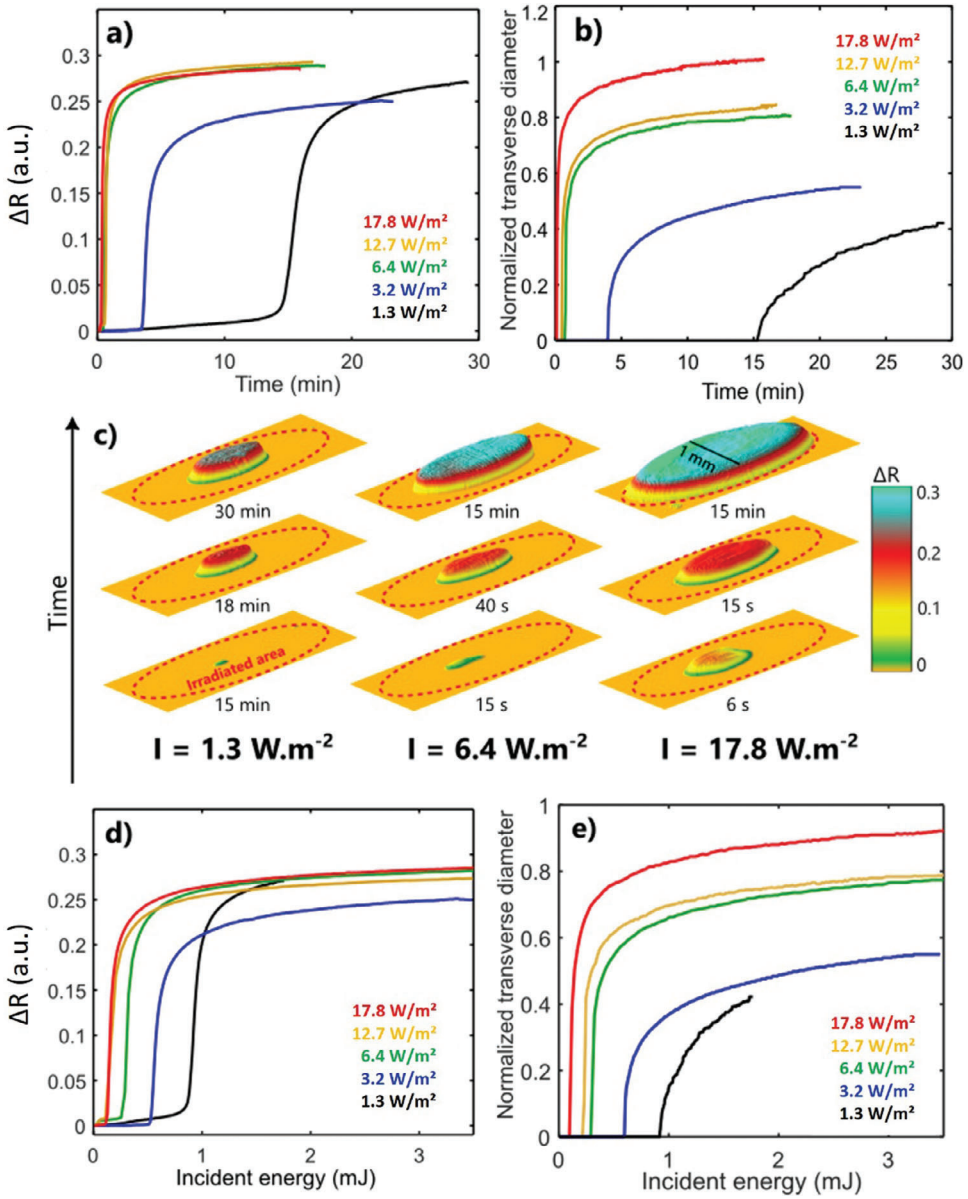

Figure 5. a): SPR reflectivity as a function of time for different irradiances b): Evolution with time of the normalized transverse diameter of the spot (normalization by irradiated area diameter: see Figure S4, Supporting Information) **c**): 3D view of polymer spot growth for different irradiances. d): SPR reflectivity as a function of incident energy for different irradiances. e): Evolution with the energy of the normalized transverse diameter of the spot. In Figures (d) and (e), the incident energy was calculated by multiplying the irradiance by the irradiation time.

At high irradiance, the threshold time is expected to be linear with the inverse of irradiance as incident light removes oxygen in the irradiated zone proportionally with time. At low irradiance, diffusion of oxygen from the edges becomes a limiting factor and the threshold time diverges as seen in Figure 6a. On the other hand, the polymerization rate K_v (Figure 6b), increases linearly up to an irradiance of 6.5 W m^{-2}, beyond which the maximum rate stabilizes. A dependence between K_v and irradiance is to be expected, as the rate of initiation is directly linked to the number of absorbed photons which is proportional to the total number of photons. The saturation of K_v can be explained by an absorption limit of the PI above a certain irradiance.

2.2. Effect of MB Concentration

The aim is to determine whether NF and bulk polymerization follow the same dependency with the concentration of photoinitiator. One question is the effective MB concentration on the gold surface, which could be different from the bulk due to a greater affinity of the MB for the gold surface than for the monomer. To answer these questions, we carried out a study of NFPP kinetics using formulations with different MB concentrations (**Table 1**), while maintaining a constant irradiance of 6.4 W m^{-2}. The results of this study are shown in **Figure 7**.

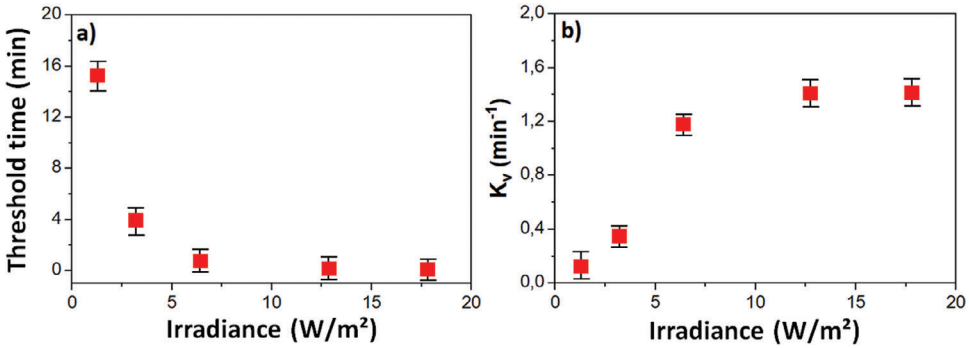

Figure 6. a) Evolution of the threshold time as a function of the irradiance. b) Polymerization rate K_v as a function of incident irradiance.

Table 1. Formulations composition used in the NFPP study.

Formulation	MB [mM]	MDEA [mM]	Monomer
F1	2,10	469,13	PETA
F2	7,00	469,13	PETA
F3	17,50	469,13	PETA

At a concentration of MB of 2.1 mM, the NFPP reaction does not start, even after 20 min of irradiation (Figure 7a). This clearly demonstrates that NFPP is dependent on PI concentration. By increasing the concentration to 7 mM, the NFPP reaction is triggered after 2 min and 30 s of irradiation. More than doubling this concentration (formulation F3), only slightly affected NFPP kinetics, suggesting a concentration limit seems to have been reached (Figure 7c,d). This observation can be explained by previous simulations of the enhancement factor (Figure 3), which show that high MB concentration induces a reduction in the NF enhancement factor. In other words, although increasing MB concentration would normally accelerate polymerization kinetics, the fact that it also decreases the enhancement factor cancels the impact on kinetics. Looking at the vertical growth (Figure 7a), we see that increasing MB concentration does not significantly impact the final thickness of the polymer spots. As for lateral growth (Figure 7b), increasing MB concentration leads to an enlargement of the polymer spot diameter as it promotes more rapid oxygen consumption in the near field.

We compare the threshold times measured in such near-field plasmonic excitation with a far-field experiment where a thin film (100 microns) of F_{633} between two glass slides was illuminated at a similar irradiance (Figure 7c). In this case, the threshold time is defined as the time required to obtain insoluble polymer between the glass slides. Overall, threshold times measured with

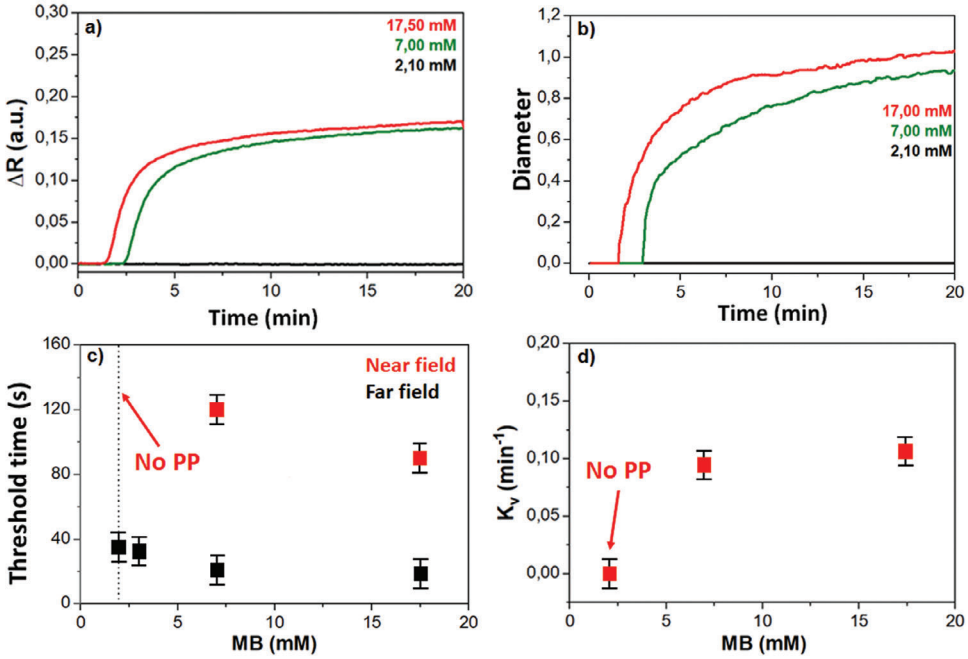

Figure 7. Evolution as a function of MB concentration of a): SPR Reflectivity, b): Normalized transverse spot diameter, c): threshold time (comparison of threshold times in near field (incident irradiance: 6.4 W m^{-2}) and far-field (incident irradiance: 6.7 W m^{-2}), d): NFPP rate constants (K_v, calculated at the start of the reaction).

Table 2. Compositions of the formulations used in the MDEA effect study.

Formulation	MB [mM]	MDEA [mM]	PETA [mM]
F1'	10,80	171,10	3878,30
F2'	10,80	256,50	3839,80
F3'	10,50	504,50	3727,10

a far-field excitation are lower by a factor of 5 compared to the one obtained in the near field, for all MB concentrations. What's more, photopolymerization is not possible for the lowest MB concentration, whereas it is possible with a far-field excitation. This result is surprising if we remember that the plasmonic field enhancement factor is greater than 10. But, as discussed previously, the inhibitory role of oxygen plays a major role in these reactions. In the far field configuration, irradiation is performed over the entire volume of the formulation, and the laminated configuration between 2 glass plates prevents oxygen renewal. Under these conditions, the medium is homogeneously depleted throughout the irradiated volume, with no possibility of replenishment, enabling the polymerization threshold to be reached, even under the least favorable conditions, for the lowest MB concentration. On the other hand, in the SPR configuration, the irradiated zone in which competition between inhibition and polymerization occurs has a very small volume (a few hundred μm^3) compared with the total volume of the formulation. Under these conditions, the inhibitor consumed at the metal surface is continuously replenished from the remaining volume of the formulation, in which it remains at its initial concentration. The formulation thus constitutes a reservoir of inhibitors that cannot be consumed within the reaction time. In the end, this explains the delay observed in the case of NFPP. Finally, the fact that the threshold time is reduced as a function of increasing MB concentration between 7 and 17 mM in the case of near-field excitation and much less in the far-field configuration confirms that the system response is linked to the MB concentration in the formulation and not over-concentration on the gold surface, as this effect would be identical in both experiments.

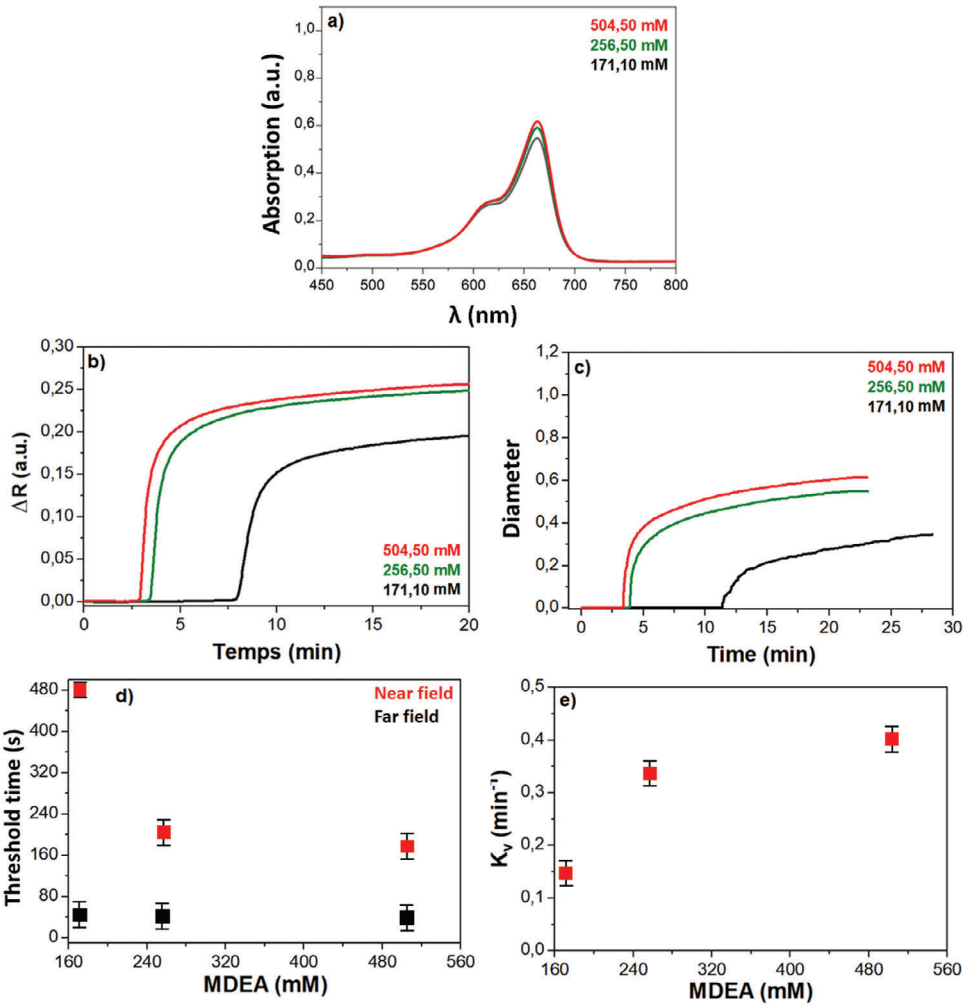

Figure 8. a): UV–vis spectra of F_{633} formulations at different MDEA concentrations. b): Evolution of SPR reflectivity, c): evolution of normalized transverse diameter (mm), d): threshold time variation as a function of MDEA concentration (comparison of threshold times in near field (incident irradiance: 6.4 W m^{-2}) and far-field (incident irradiance: 6.7 W m^{-2}), e): NFPP rate constants (measured at the start of the reaction) as a function of MDEA concentration.

2.3. Effect of MDEA Concentration

To demonstrate the purely photochemical aspect of this NF polymerization reaction, we prepared a formulation by removing the MDEA (F_{633}-MDEA) and irradiating it at the maximum irradiance of 17.8 W m^{-2}. In this case, no NFPP reaction was observed (Figure S5, Supporting Information), confirming that the reaction occurs solely by a photochemical mechanism, excluding thermal[22] or electronic processes.[23] We also look at different concentrations of MDEA. The composition and UV–visible spectra of the different formulations are shown in **Table 2** and **Figure 8a** respectively.

Increasing the amount of MDEA does not significantly influence the spectral properties of MB and thus the absorption properties at 633 nm of the formulation are the same for all formulations. The monitoring of NFPP as a function of MDEA concentration is illustrated in Figure 8b. It shows that MDEA concentration affects threshold time and NFPP kinetics. At lower MDEA concentrations, the reaction is slower, confirming the role of MDEA in initiating the PP reaction. The NFPP threshold time decreases with increasing MDEA concentration (Figure 8d in red), and the maximum polymerization rate (K_v) also increases with increasing MDEA concentration (Figure 8e). From 256 mM onward, threshold time and K_v tend toward a constant value.

As before, we also compare the effect of MDEA concentration on the threshold times in near-field and far-field excitation (Figure 8d in black). The dependence of NFPP on MDEA concentration is similar to the one observed with MB concentration. Threshold times are, for all concentrations, greater in the near field, despite the enhancement expected in this configuration. This result can again be interpreted as oxygen consumption acting as a polymerization inhibitor in both macroscopic and nanolayer environments, with the possibility of replenishment by diffusion during irradiation in the near field configuration. These observations also exclude an over-concentration effect of MDEA in the zone corresponding to the near field. Such an effect could have occurred considering the affinity of amines for gold surfaces. We show here that this effect is not significant. This conclusion can be extended to other studies involving systems with MDEA, such as the Eosin-Amine system widely used for NFPP.[7,11,24]

3. Conclusion

In this work, we proposed a novel dual-wavelength SPR imaging instrument for monitoring near-field photopolymerization at the nanoscale and in real time. Acquired kinetics revealed how polymer growth in the near-field, both in terms of threshold energy and polymerization rate, and the dependency on irradiance. We observed that the lateral polymer diameter is strongly influenced by irradiance, while its maximum thickness remains mostly insensitive to irradiance, as it is limited by the extension of the plasmonic evanescent field. Increasing the concentration of the photoinitiator shows a saturation effect on the kinetics that was explained by a decrease in the enhancement factor of the plasmonic near-field. We also observed that the kinetics of near-field photopolymerization differ from the one obtained in the far-field as polymerization undergoes a more pronounced inhibition of the reaction due to oxygen diffusion. This diffusion is more pronounced in near-field where only a very confined volume of the formulation is irradiated, in contrast to the situation in far-field where the entire volume is exposed to light. This work shows the capability of this experimental configuration for investigating photopolymerization at the nanoscale. Knowledge and control over photopolymerization reactions at this scale would lead to a better understanding of the properties of the polymer nanolayers formed and their potential use in nanophotonic or sensor applications.

4. Experimental Section

The Dual-Wavelengths SPRI Instrument: Briefly, the setup is based on a dual-wavelength illumination (Figure 1c) of the gold film sample: a He-Ne laser (632.8 nm) triggers the photopolymerization through the surface plasmon evanescent field and a low-irradiance, low coherence LED (610 nm) is used to monitor the shift of the surface plasmon resonance. The irradiance of the light coming from the LED at 610 nm on the sample is 100x lower compared to the irradiance of the laser source used to excite the plasmon at 633 nm. The angle of incidence on the sample is tuned to the minimum reflectivity of the He-Ne laser photopolymerization wavelength to maximize the plasmonic field intensity. At this working point, the sensitivity of the SPR is close to zero. Using the second wavelength (LED) for interrogation, positioned on the slope of the resonance, allows for recovery of full sensitivity, down to 10^{-6} RIU. It also avoids all problems of saturation and speckle noise in the acquired images. The instrument is based on a Kretschmann configuration operating in intensity modulation[15] (Data S1 and Figure S1, Supporting Information). In this study, the temporal resolution is ≈1.7 s.

Photopolymerizable Formulation: The photopolymerizable formulation (F_{633}) is composed of pentaerythritol triacrylate (PETA, Sigma Aldrich) as a monomer (RI = 1.48), and a Norrish II-type PI system consisting of a mixture of methylene blue (MB, Sigma Aldrich) and N-methyl diethanolamine (MDEA, Sigma Aldrich).

Supporting Information

Supporting Information is available from the Wiley Online Library or from the author.

Acknowledgements

A.K. and L.L. contributed equally to this work. O.S. and J.M. acknowledge ANR for funding (POPCORN grant numbers ANR-19-CE19-0012 and SURIMI ANR-18-CE04-0010). This work of the Interdisciplinary Institute HiFunMat, as part of the ITI 2021–2028 program of the University of Strasbourg, CNRS, and Inserm, was supported by IdEx Unistra (ANR-10-IDEX-0002), SFRI (STRAT'US project, ANR-20-SFRI-0012) under the framework of the French Investments for the Future Program.

Conflict of Interest

The authors declare no conflict of interest.

Data Availability Statement

The data that support the findings of this study are available from the corresponding author upon reasonable request.

Keywords

near-field photopolymerization, Plasmonic, SPR imaging, Surface Plasmon Resonance

Received: March 9, 2024
Revised: May 8, 2024
Published online:

[1] M. I. Stockman, *Opt. Express* **2011**, *19*, 22029.
[2] F. Kameche, W. Heni, S. Telitel, L. Vidal, S. Marguet, L. Douillard, C. Fiorini-Debuisschert, R. Bachelot, O. Soppera, *J. Phys. Chem. C* **2021**, *125*, 8719.
[3] F. Kameche, W. Heni, S. Telitel, D. Ge, L. Vidal, F. Dumur, D. Gigmes, J. Lalevee, S. Marguet, L. Douillard, *Mater. Today* **2020**, *40*, 38.
[4] J. Tang, K. Gao, Q. Ou, X. Fu, S.-Q. Man, J. Guo, Y. Liu, *Spectrochim. Acta, Part A* **2018**, *191*, 513.
[5] C. Zhan, X.-J. Chen, J. Yi, J.-F. Li, D.-Y. Wu, Z.-Q. Tian, *Nature Reviews Chemistry* **2018**, *2*, 216.
[6] A. Khitous, C. Molinaro, S. Gree, K. Haupt, O. Soppera, *Adv. Mater. Interfaces* **2023**, *10*, 2201651.
[7] A. Khitous, C.-F. Lin, F. Kameche, H.-W. Zan, J.-P. Malval, D. Berling, O. Soppera, *ACS Appl. Nano Mater.* **2021**, *4*, 8770.
[8] D. Ge, A. Issa, S. Jradi, C. Couteau, S. Marguet, R. Bachelot, *Photonics research* **2022**, *10*, 1552.
[9] A. Khitous, C. Molinaro, C. Thomas, K. Haupt, O. Soppera, *Sensors* **2023**, *23*, 3995.
[10] V. Chegel, M. J. Whitcombe, N. W. Turner, S. A. Piletsky, *Biosens. Bioelectron.* **2009**, *24*, 1270.
[11] C. Deeb, C. Ecoffet, R. Bachelot, J. Plain, A. Bouhelier, O. Soppera, *J. Am. Chem. Soc.* **2011**, *133*, 10535.
[12] J. Jatschka, A. Dathe, A. Csáki, W. Fritzsche, O. Stranik, *Sensing and bio-sensing research* **2016**, *7*, 62.
[13] I. Kaminska, T. Maurer, R. Nicolas, M. Renault, T. Lerond, R. Salas-Montiel, Z. Herro, M. Kazan, J. Niedziolka-Jönsson, J. Plain, *J. Phys. Chem. C* **2015**, *119*, 9470.
[14] O. Tokel, F. Inci, U. Demirci, *Chem. Rev.* **2014**, *114*, 5728.
[15] *Surface Plasmon Resonance Based Sensors*, (Ed.: J. Homola), Springer Series on Chemical Sensors and Biosensors, Springer, Berlin, Heidelberg, **2006**, Vol. *4*.
[16] J. Moreau, L. Lartigue, *Photoniques* **2022**, 46.
[17] E. Kretschmann, *Zeitschrift für Physik A Hadrons and nuclei* **1971**, *241*, 313.
[18] M. Besbes, SimPhotonics Matlab toolbox, https://github.com/SimPhotonicsFMM.
[19] A. Sereda, J. Moreau, M. Canva, E. Maillart, *Biosens. Bioelectron.* **2014**, *54*, 175.
[20] P. Lecaruyer, E. Maillart, M. Canva, J. Rolland, *Appl. Opt.* **2006**, *45*, 8419.
[21] S. C. Ligon, B. Husár, H. Wutzel, R. Holman, R. Liska, *Chem. Rev.* **2014**, *114*, 557.
[22] M. Fedoruk, M. Meixner, S. Carretero-Palacios, T. Lohmüller, J. Feldmann, *ACS Nano* **2013**, *7*, 7648.
[23] T. Ding, J. Mertens, A. Lombardi, O. A. Scherman, J. J. Baumberg, *ACS Photonics* **2017**, *4*, 1453.
[24] H. I. El Ahrach, R. Bachelot, A. Vial, G. Lerondel, J. Plain, P. Royer, O. Soppera, *Phys. Rev. Lett.* **2007**, *98*, 107402.